

Replace this line with article main subject (see Index Terms below)

Spintronic Neuron Using a Magnetic Tunnel Junction for Low-Power Neuromorphic Computing

Steven Louis^{1*}, Hannah Bradley^{2*}, Cody Trevillian^{2*}, Andrei Slavin^{2**}, and Vasyly Tyberkevych^{2*}

¹Department of Electrical and Computer Engineering, Oakland University, Rochester, MI 48309, USA

²Department of Physics, Oakland University, Rochester, MI 48309, USA

*Member, IEEE

**Fellow, IEEE

Received xxxx 00, 0000, revised xxxx 00, 0000, published xxxx 00, 0000, current version xxxx 00, 0000 (Dates will be inserted by IEEE; “published” is the date the accepted preprint is posted on IEEE Xplore®; “current version” is the date the typeset version is posted on Xplore®).

Abstract—This paper proposes a novel spiking artificial neuron design based on a combined spin valve/magnetic tunnel junction (SV/MTJ). Traditional hardware used in artificial intelligence and machine learning faces significant challenges related to high power consumption and scalability. To address these challenges, spintronic neurons, which can mimic biologically inspired neural behaviors, offer a promising solution. We present a model of an SV/MTJ-based neuron which uses technologies that have been successfully integrated with CMOS in commercially available applications. The operational dynamics of the neuron are derived analytically through the Landau-Lifshitz-Gilbert-Slonczewski (LLGS) equation, demonstrating its ability to replicate key spiking characteristics of biological neurons, such as response latency and refractive behavior. Simulation results indicate that the proposed neuron design can operate on a timescale of about 1 ns, without any bias current, and with power consumption as low as 50 μ W.

Index Terms— Insert keywords here

I. INTRODUCTION

Recent advancements in artificial intelligence (AI) and machine learning (ML) have been remarkable [Wu 2023]. However, traditional hardware used for AI applications often faces challenges such as high power consumption and significant costs [Strubell2020]. To mitigate these problems, recent research has proposed utilizing spintronic spiking neurons for AI and ML tasks [Khymyn 2018, Liu 2020, Louis 2022, Mitrofanova 2022, Ovcharov 2022, Bradley 2023, Rodrigues 2023, Manna 2023, Sengupta 2016, Cai 2019]. Spintronic spiking neurons are promising because they can exhibit biologically inspired features such as response latency, refractive behavior, and inhibition—all within a single component [Bradley 2023]. These characteristics have the potential to enhance the design of AI hardware.

In this article, we propose to use a combined spin valve (SV) and magnetic tunnel junction (MTJ) to form a biologically plausible artificial spiking neuron. Spin valves and MTJs have been extensively manufactured for commercial purposes. For over two decades, spin valves and MTJs were widely used as the read head for magnetic hard drives [Alzate 2015]. More recently, MTJs have been used in magnetoresistive random access memory (MRAM) as a non-volatile memory element. In MRAM, MTJs have been embedded in CMOS with a process length as small as 14 nanometers [Edelstein 2020]. Given the longstanding practical implementation of SV/MTJs, developing a spintronic spiking neuron based on these technologies has the potential to be highly advantageous.

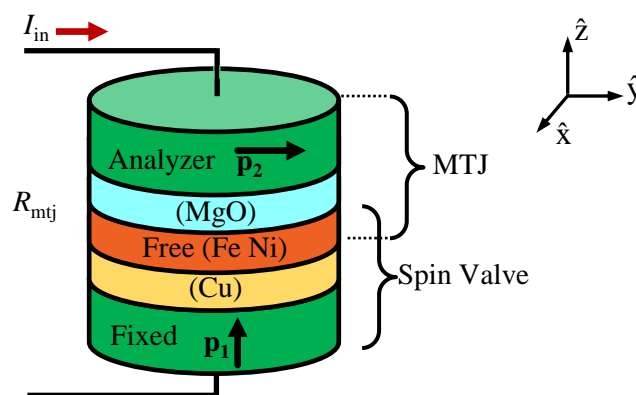


Fig. 1. Schematic of the SV/MTJ neuron. The lower layers of the stack constitute a spin valve, while the upper layers constitute a magnetic tunnel junction. The input current flows through the stack as labeled, and R_{mtj} is the resistance of the stack.

This paper presents a potential design of an SV/MTJ combination that can act as a spintronic spiking neuron. We demonstrate that the Landau-Lifshitz-Gilbert-Slonczewski (LLGS) equation for this particular configuration of SV/MTJ can be converted to the artificial neuron equation (ANE), which describes the dynamics of the artificial neuron [Bradley 2023]. In addition, this paper will present basic characteristics of the SV/MTJ neuron.

Overall, this proposed design of an SV/MTJ combination as a biologically plausible artificial spiking neuron has the potential to advance the field of AI and ML by providing a readily realizable hardware option for biologically realistic spintronic neurons.

Corresponding author: Steven Louis (SLouis@oakland.edu).

Digital Object Identifier 10.1109/LMAG.2020.Doi Number

II. NEURON DESIGN AND MATHEMATICAL MODEL

The proposed neuron is composed of a stack of ferromagnetic layers separated by spacer layers. A sketch of the proposed stack is shown in Fig. 1. The bottom of the stack is a spin valve, consisting of a fixed layer, a copper spacer layer, and a free layer. The fixed layer has a magnetic anisotropy that keeps its magnetization oriented out-of-plane (labeled \mathbf{p}_1 in the figure). The top of the stack is a magnetic tunnel junction that extracts the signal. This MTJ includes an analyzer layer with magnetization oriented in-plane (labeled \mathbf{p}_2 in the figure), and is separated from the free layer by an MgO spacer.

The SV/MTJ neuron operates as follows. An electric current, I_{in} , flows through the stack and exerts a spin-transfer torque on the free layer magnetization. This electric current can be considered as an input to the neuron. The dynamics of the free layer magnetization under the influence of I_{in} can be modeled in the macrospin approximation by the Landau–Lifshitz–Gilbert–Slonczewski (LLGS) equation [Slavin, 2009]:

$$\frac{d\mathbf{m}}{dt} = |\gamma|\mathbf{B}_{\text{eff}} \times \mathbf{m} + \alpha_G \mathbf{m} \times \frac{d\mathbf{m}}{dt} + \sigma_j I_{\text{in}} \mathbf{m} \times \mathbf{m} \times \mathbf{p}_1. \quad (1)$$

In this equation, \mathbf{m} is the unit magnetization of the free layer, \mathbf{p}_1 is the unit magnetization of the polarizer, γ is the gyromagnetic ratio, \mathbf{B}_{eff} is the effective magnetic field, α_G is the Gilbert damping parameter, and σ_j is the spin torque coefficient. The effective field is $\mathbf{B}_{\text{eff}} = \mathbf{B}_{\text{ext}} + \mathbf{B}_A + \mathbf{B}_d$, where \mathbf{B}_{ext} is an external magnetic field, \mathbf{B}_A is the field due to magnetic anisotropy in the free layer, and \mathbf{B}_d is the demagnetizing field. The spin torque coefficient is given by $\sigma_j = |\gamma|\hbar\mu_0\eta_0/(2B_d eV)$, where \hbar is the reduced Planck constant, η_0 is the spin polarization efficiency, M_s is the free layer saturation magnetization, e is the fundamental electric charge, and V is the volume of the free layer.

The output of the neuron is the resistance R_{mtj} across the SV/MTJ stack, which is given by $R_{\text{mtj}} = R_0 + \Delta R(\mathbf{m} \cdot \mathbf{p}_2)$, where \mathbf{p}_2 is the unit magnetization of the analyzer layer, ΔR is the amplitude of MTJ resistance change, and R_0 is the average MTJ resistance.

In the simulations that follow, we have chosen the polarizer magnetization to have an out-of-plane orientation ($\mathbf{p}_1 = \hat{\mathbf{z}}$). The analyzer layer magnetization (\mathbf{p}_2) was selected to have an in-plane orientation. The free layer is considered isotropic ($\mathbf{B}_A = 0$) and is subject to a demagnetization field $\mathbf{B}_d = 1$ T in the $-\hat{\mathbf{z}}$ direction, as well as an external field \mathbf{B}_{ext} with a magnitude of 1 mT in the $-\hat{\mathbf{x}}$ direction. This configuration resembles one that was previously fabricated and characterized in an experimental study [Houssameddine, 2007]. It was chosen because the free layer magnetization is in-plane at equilibrium while exhibiting out-of-plane precession. With this setup, the derivation of the ANE can be clearly demonstrated. In addition, other geometries of MTJs can also serve as spintronic neurons, as shown in simulations by [Rodrigues, 2023]. The following sections aim to inspire further research within the broader spintronics and MRAM community to develop neuromorphic hardware based on spiking neurons that can be integrated with CMOS and other conventional computing platforms.

Additional simulation parameters include $\gamma = 2\pi \times 28$ GHz/T, $\alpha_G = 0.1$, $\eta_0 = 0.35$, $V = 3 \times 10^4$ nm³, $R_0 = 1500$ Ω , and

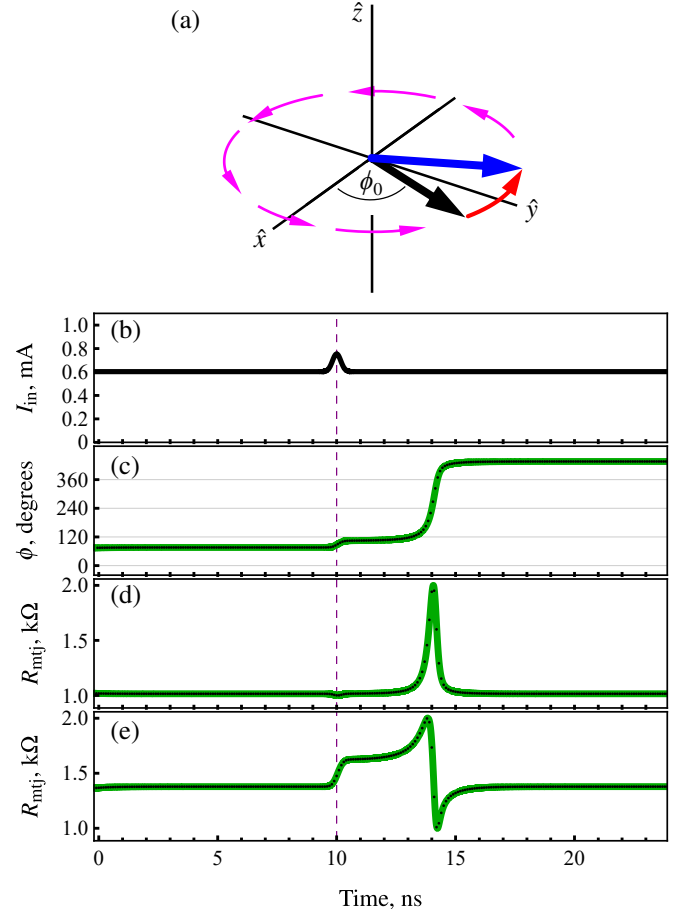


Fig. 2. Simulation results illustrating the magnetization dynamics and output resistance of the SV/MTJ neuron. (a) Rotation of the free layer magnetization layer in the x - y plane. The black arrow represents the steady-state magnetization angle $\phi_0 = 73^\circ$, the blue arrow represents the magnetization after impulse with a phase angle of 111° , the red arrow indicates the temporary shift due to a brief increase in input current, and the magenta arrows depict the full 360° rotation of the magnetization. (b) Input current I_{in} for the system (c) Evolution of ϕ , the magnetization azimuthal angle, with time. Green curves are results from LLGS simulations, while gray dashed lines are results of ANE simulations. (d) Change in R_{mtj} with time for $\mathbf{p}_2 = \hat{\mathbf{y}}$. (e) Change in R_{mtj} with time for $\mathbf{p}_2 = \hat{\mathbf{x}}$.

$\Delta R = 500$ Ω . These values were chosen because they are typical for SV/MTJs. Please note that although there is a resistance associated with the spin valve portion of the stack, it is negligible compared to the resistance of the MTJ analyzer. We also assumed that \mathbf{p}_2 remained pinned in a specific direction during neuron operation.

III. DERIVATION AND SIMULATION OF ARTIFICIAL NEURON EQUATION

In this section, it will be shown that the ANE can be derived from (1). This derivation begins by performing a scalar product between

$\frac{\partial m}{\partial \theta}$, $\frac{\partial m}{\partial \phi}$ and $\frac{dm}{dt}$, yielding a pair of equations:

$$\frac{d\theta}{dt} = \omega_B \sin \phi + \alpha_G \cos \theta d\phi - \sigma_j I_{in} \cos \theta, \quad (2a)$$

$$\frac{d\phi}{dt} = -\omega_M \sin \theta - \omega_B \tan \theta \cos \phi - \alpha_G \frac{1}{\cos \theta} d\theta. \quad (2b)$$

In these equations, ϕ is the azimuthal angle of \mathbf{m} , θ is the out-of-plane angle of \mathbf{m} , $\omega_B = |\gamma|B_{ext}$, and $\omega_M = |\gamma|B_d$.

We assume that during the operation of the SV/MTJ neuron, the magnetization of the free layer stays almost in-plane, which means we can use the small angle approximation for θ . Using this approximation, substituting equation (2a) into equation (2b), and ignoring the nonlinear terms, leads to the following equation:

$$\frac{d\phi}{dt} = -\omega_M \theta - \omega_B \theta \cos \phi - \alpha_G \omega_B \sin \phi. \quad (3)$$

This equation allows us to solve for θ :

$$\theta = -\frac{\frac{d\phi}{dt} + \alpha_G \omega_B \sin \phi}{\omega_M},$$

where we have neglected the $\omega_B \cos \phi$ term in the denominator since ω_M is much larger than ω_B . After taking the time derivative of θ , we can equate it with equation (2a). From this, we can directly solve for the artificial neuron equation:

$$\frac{1}{\omega_M} \frac{d^2 \phi}{dt^2} + \alpha_G \frac{d\phi}{dt} + \omega_B \sin \phi = \sigma_j I_{in}. \quad (4)$$

Similar artificial neuron equations have been derived in previous research for various spintronic devices, including antiferromagnetic neurons [Khymyn 2018], synthetic antiferromagnetic oscillators [Liu 2020], optically initialized antiferromagnetic-heavy metal heterostructures [Mitrofanova 2022], a spin Hall nano-oscillator [Ovcharov 2022], and spin superfluid Josephson oscillators [Crotty 2010, Schneider 2018].

For this system, there is a threshold current, I_{th} , as in spin-torque-nano-oscillators [Slavin 2009]. When the input current $I_{in} > I_{th}$, the free layer magnetization will precess about \mathbf{B}_{eff} [Houssameddine 2007]. For the geometry considered here, there will be an out-of-plane rotation for steady-state currents above I_{th} [Houssameddine 2007].

When there is no input current ($I_{in} = 0$), \mathbf{m} will be aligned with \mathbf{B}_{ext} , along the \hat{x} direction. When the input current is positive, but $I_{in} \leq I_{th}$, the free layer magnetization will remain stationary in the $\hat{x} - \hat{y}$ plane with a phase angle ϕ less than the threshold phase of 90° . When the phase is $\phi = 90^\circ$, the threshold current can be calculated from (4), and is

$$I_{th} = \frac{\omega_B}{\sigma_j}. \quad (5)$$

With the parameters considered above, the threshold voltage is $I_{th} \sim 0.622$ mA.

The magnetization dynamics of the system are illustrated in Fig. 2 through the simulation of equation (1). Additionally, we demonstrate that equation (4) provides a reasonable approximation of the LLGS for this device geometry.

In this simulation, the input current consists of a bias DC current, I_{bias} , and a temporary impulse current, i_p , so that $I_{in} = I_{bias} + i_p$. For this setup, I_{bias} is set to 0.6 mA. It is important to note that this is a sub-threshold current, meaning $I_{in} < I_{th}$. At this current level,

spin transfer torque causes the free layer magnetization to rotate in the $\hat{x} - \hat{y}$ plane, forming an angle $\phi_0 = 73^\circ$ with the \hat{x} axis. This is depicted in Fig. 2(a), where the black arrow represents the free layer magnetization under the influence of a constant 0.6 mA current. The same behavior is shown in Fig. 2(b) and Fig. 2(c) during the first 9 ns of the simulation. In Fig. 2(b), the black line represents the input current amplitude, while the green lines in Fig. 2(c), (d), and (e) show the results from simulating equation (1). The black dots in Fig. 2(c)-(e) represent the results from simulating equation (4).

At time $t = 10$ ns in the simulation, the input current I_{in} briefly increases to approximately 0.75 mA, as shown in Fig. 2(b). In response to this perturbation, the free layer magnetization is temporarily pushed from ϕ_0 past 90° to 111° , as indicated by the red arrow in Fig. 2(a). Following a delay of about 4 ns, the free layer magnetization undergoes a full 360° rotation in the $x - y$ plane before returning to ϕ_0 . This rotation is depicted by the magenta arrows in Fig. 2(a) and by the green line in Fig. 2(c) around $t = 14$ ns, when the phase angle increases to 433° .

The output resistance R_{mj} , with \mathbf{p}_2 pinned in the \hat{y} direction, is shown in Fig. 2(d). With this analyzer configuration, the resistance of the structure momentarily increases from 1 k Ω to 2 k Ω , showing a spiking response characteristic of previous studies [Bradley 2023]. Alternatively, if \mathbf{p}_2 is pinned in the \hat{x} direction, the output resistance changes as shown in Fig. 2(e).

The duration of the spiking response in Fig. 2(d) is on the order of 1 ns. This is substantially faster than the response speed of a biological neuron (~ 1 ms), but slower than the speed of an antiferromagnetic neuron (~ 1 ps).

It is important to note that Figs. 2(c)-(e) display results from two different simulations. The black dots represent the simulation using the ANE in equation (4), while the green line represents the simulation of the LLGS equation in equation (1). From these results, it is clear that, for this set of simulation parameters, the ANE provides a valid approximation of the LLGS.

IV. SIMULATION OF SV/MTJ NEURON CHARACTERISTICS

In the previous section, we demonstrated that the behavior of SV/MTJ can be effectively modeled using ANE. This finding suggests that the characteristics previously established for antiferromagnetic neurons, such as response latency, refraction, inhibition, variable spiking modes, and adherence to the ‘‘all-or-nothing’’ law, are also applicable to SV/MTJ neurons [Bradley 2023].

In biological neural networks, varying response latency based on input amplitude is a fundamental mechanism for learning. The variable response latency of SV/MTJ, as determined from simulating (1) with $\mathbf{p}_2 = \hat{y}$ and $I_{th} = 0.6$ mA, is illustrated in Fig. 3(a) and (b). Fig. 3(a) shows a simulated input current with a bias of approximately 0.6 mA, along with two current impulses: the first at $t = 5$ ns and the second at $t = 15$ ns. Note that the second impulse is larger than the first. The corresponding output response, represented by R_{mj} of the SV/MTJ, is depicted in Fig. 3(b). In Fig. 3(b), the response latency for the first, smaller impulse is 3

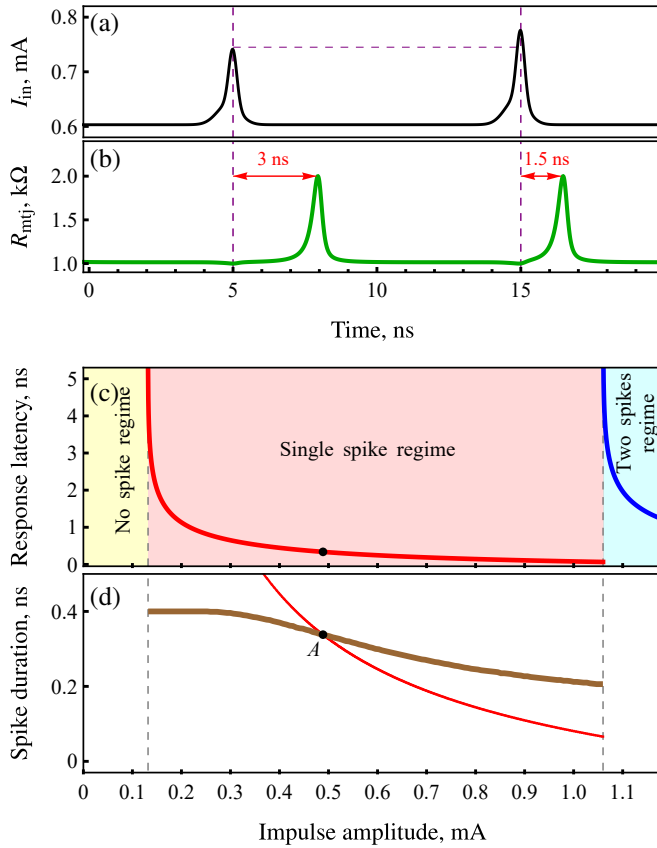


Fig. 3. (a) Simulated input current with a bias of approximately 0.6 mA, including two current impulses at $t = 5$ ns and $t = 15$ ns. (b) Corresponding output response R_{mjt} of the SV/MTJ, showing variable response latency of 3 ns for the first impulse and 1.5 ns for the second, larger impulse. (c) Simulation results for response latency across impulse amplitudes ranging from 0 to 1.2 mA, with regions indicating no spike (yellow), single spike (red), and two spikes (blue). (d) Variation in spike duration (brown line) and response latency (red curve), and point 'A' where latency and spike duration intersect.

ns, while the response latency for the second, larger impulse is 1.5 ns. This demonstrates that the response latency shortens as the input current impulse amplitude increases, as previously seen for antiferromagnetic neurons [Bradley 2023].

To further investigate the response latency in this system, a series of simulations were conducted with impulse amplitudes (i_p) ranging from 0 to 1.2 mA. The simulation results are presented in Fig. 3(c). As illustrated by the yellow region, the SV/MTJ neuron does not spike for impulse amplitudes below 0.15 mA. For impulse amplitudes between 0.15 mA and 1.06 mA, the neuron generates a single spike, with the response latency depicted by the red curve in the red region. For impulse amplitudes exceeding 1.06 mA, the neuron produces two spikes, with the inter-spike period indicated by the blue curve in the blue region. In the single spike regime, it is evident that smaller impulse amplitudes result in longer response latencies, whereas larger impulse amplitudes lead to shorter response latencies.

In addition to the change in response latency, it is important to note that the amplitude and spike duration of the SV/MTJ output resistance in Fig. 3(b) remain nearly constant, even as the input amplitude varies. The brown line in Fig. 3(d) shows how the spike duration changes with i_p , while the red curve represents the response latency. For longer response latencies, the spike duration stays relatively consistent. However, when the impulse amplitude is strong, the neuron generates a spike almost immediately after the input, causing the response latency to shorten. When the response latency becomes shorter than the spike duration (as seen at point 'A' in Fig. 3(d)), the spike duration decreases. In essence, the spike duration decreases when the neuron spikes immediately after the impulse.

Figure 4, which was also obtained through simulation, characterizes the response of the SV/MTJ neuron to bias currents that vary from 0 to 0.7 mA. How the different spiking regimes vary with bias current is shown in Figure 4(a). The region shaded yellow shows where the SV/MTJ neuron does not spike. The red region shows where there is a single spike. The blue region shows where there are multiple spikes. As expected, the region above I_{th} has multiple spikes without any impulse current. Several other observations about this figure are notable. First, higher impulse currents are required to generate a spike for lower bias currents. A wider range of impulse currents can generate a spike for lower bias currents. Most notably, according to these simulations, it is possible to induce spikes with zero bias current.

Figure 4(b) shows how the power consumption of the SV/MTJ neuron varies with changing bias current, assuming a time per synaptic operation is conservatively estimated to be 20 ns and a p_2 that is aligned with ϕ_0 . In this figure, the green region represents the steady-state power consumption due to the bias current, while the red region indicates the dynamic power consumption, which includes both the impulse current and the changing resistance of the neuron. From the figure, it is clear that the power consumption remains below 0.3 mW for high bias currents. For lower bias currents, the power consumption decreases to approximately 50 μ W. Additionally, while the dynamic power consumption increases with lower bias currents, it does not reach the levels observed at higher bias currents.

V. CONCLUSION

In this paper, we introduced a novel approach to neuromorphic computing by developing an artificial neuron based on a combination of a spin valve and a magnetic tunnel junction. We analytically derived the artificial neuron equation from the Landau-Lifshitz-Gilbert-Slonczewski equation, and demonstrated through simulations that the ANE serves as a reliable approximation of the LLGS for this specific SV/MTJ design. Our simulation results further indicate that the proposed neuron can operate on a timescale of about 1 ns, without any bias current, achieving power consumption as low as 50 μ W. These findings underscore the potential of SV/MTJ neurons to offer a low-power, scalable, and biologically plausible solution for neuromorphic computing. Given that both spin valves and magnetic

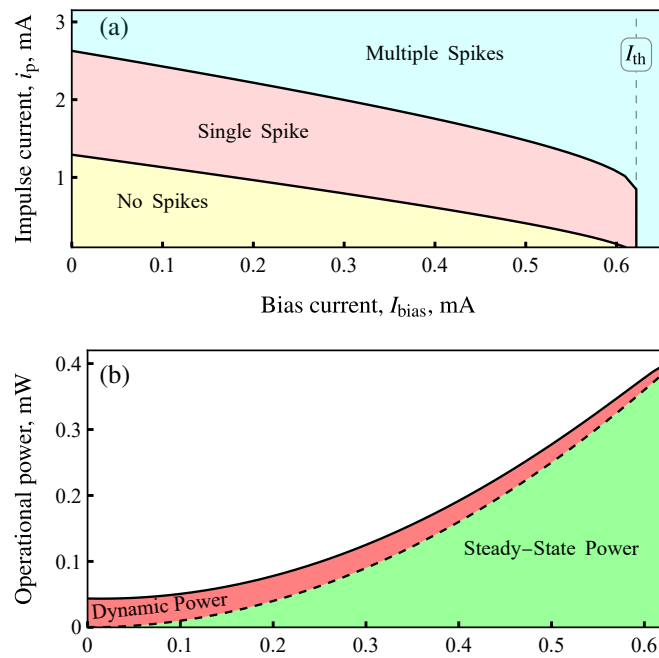


Fig. 4. Simulation results characterizing the response of the SV/MTJ neuron to varying bias currents. (a) The spiking regimes of the neuron. The yellow region indicates no spikes, the red region indicates a single spike, and the blue region indicates multiple spikes. I_{th} indicated by a dashed line. (b) Power consumption of the neuron. The green region represents steady-state power consumption, while the red region shows dynamic power consumption. Assumes 20 ns per synaptic operation and p_2 aligned with ϕ_0 .

tunnel junctions are well-established, commercially available technologies that can be integrated with CMOS, they present a promising avenue for practical implementation. This work lays the foundation for future research and development in spintronic neurons, which could significantly enhance the efficiency and capabilities of next-generation AI systems.

REFERENCES

- Wu, T., He, S., Liu, J., Sun, S., Liu, K., Han, Q. L., & Tang, Y. (2023). A brief overview of ChatGPT: The history, status quo and potential future development. *IEEE/CAA Journal of Automatica Sinica*, 10(5), 1122-1136.
- Strubell, E., Ganesh, A., McCallum, A. (2020, April). Energy and policy considerations for modern deep learning research. In *Proceedings of the AAAI conference on artificial intelligence* (Vol. 34, No. 09, pp. 13693-13696).
- Bradley, H., Louis, S., Trevillian, C., Quach, L., Bankowski, E., Slavin, A., Tyberkevych, V. (2023). Artificial neurons based on antiferromagnetic auto-oscillators as a platform for neuromorphic computing. *AIP Advances*, 13(1).
- Liu, Y., Barsukov, I., Barlas, Y., Krivorotov, I. N., Lake, R. K. (2020). Synthetic antiferromagnet-based spin Josephson oscillator. *Applied Physics Letters*, 116(13).
- Khymyn, R., Lisenkov, I., Voorheis, J., Sulymenko, O., Prokopenko, O., Tiberkevich, V., Akerman, J., Slavin, A. (2018). Ultra-fast artificial neuron: generation of picosecond-duration spikes in a current-driven antiferromagnetic auto-oscillator. *Scientific reports*, 8(1), 15727.
- Bradley, H., Quach, L., Louis, S., Tyberkevych, V. (2024). Antiferromagnetic artificial neuron modeling of the withdrawal reflex. *Journal of Computational Neuroscience*, 1-10.
- Alzate, J. G., Amiri, P. K., Wang, K. L. (2015). Magnetic tunnel junctions and their applications in non-volatile circuits. In *Handbook of Spintronics* (pp. 1127-1171). Springer Netherlands.

- Edelstein, D., Rizzolo, M., Sil, D., Dutta, A., DeBrosse, J., Wordeman, M., ... Worledge, D. C. (2020, December). A 14 nm embedded STT-MRAM CMOS technology. In *2020 IEEE International Electron Devices Meeting (IEDM)* (pp. 11-5). IEEE.
- Houssameddine, D., Ebels, U., Delaët, B., Rodmacq, B., Firastrau, I., Ponthenier, F., Brunet, M., Thirion, C., Michel, J. P., Prejbeanu-Buda, L., Cyrille, M. C., Redon, O., Dieny, B. (2007). Spin-torque oscillator using a perpendicular polarizer and a planar free layer. *Nature materials*, 6(6), 447-453.
- Slavin, A., Tiberkevich, V. (2009). Nonlinear auto-oscillator theory of microwave generation by spin-polarized current. *IEEE Transactions on Magnetics*, 45(4), 1875-1918.
- Mitrofanova, A., Safin, A., Kravchenko, O., Nikitov, S., Kirilyuk, A. (2022). Optically initialized and current-controlled logical element based on antiferromagnetic-heavy metal heterostructures for neuromorphic computing. *Applied Physics Letters*, 120(7).
- Ovcharov, R. V., Galkina, E. G., Ivanov, B. A., Khymyn, R. S. (2022). Spin hall nano-oscillator based on an antiferromagnetic domain wall. *Physical Review Applied*, 18(2), 024047.
- Rodrigues, D. R., Moukher, R., Luo, Y., Fang, B., Pontlevy, A., Hamadeh, A., Zeng, Z., Carpentieri, M. and Finocchio, G. Finocchio, G. (2023). Spintronic Hodgkin-Huxley-analogue neuron implemented with a single magnetic tunnel junction. *Physical Review Applied*, 19(6), 064010.
- Louis, S., Bradley, H., Slavin, A., Tyberkevych, V. (2022) Artificial Neuron Based on a Spin Torque Nano Oscillator, *Book of Abstracts for 7th International Conference on Magnonics*, C4-28.
- Schneider, M. L., Donnelly, C. A., Russek, S. E. (2018). Tutorial: High-speed low-power neuromorphic systems based on magnetic Josephson junctions. *Journal of Applied Physics*, 124(16).
- Crotty, P., Schult, D., Segall, K. (2010). Josephson junction simulation of neurons. *Physical Review E—Statistical, Nonlinear, and Soft Matter Physics*, 82(1), 011914.
- Manna, S., Medwal, R., Rawat, R. S. (2023). Reconfigurable neural spiking in bias field free spin Hall nano-oscillator. *Physical Review B*, 108(18), 184411.
- Sengupta, A., Panda, P., Wijesinghe, P., Kim, Y., Roy, K. (2016). Magnetic tunnel junction mimics stochastic cortical spiking neurons. *Scientific reports*, 6(1), 30039.
- Cai, J., Fang, B., Zhang, L., Lv, W., Zhang, B., Zhou, T., Finocchio, G., Zeng, Z. (2019). Voltage-controlled spintronic stochastic neuron based on a magnetic tunnel junction. *Physical Review Applied*, 11(3), 034015.